

## Control Scheme for a Hybrid Wind and Solar Energy Conversion System

**K.Navya**

M.Tech Student  
Department of EEE,  
Bheema Institute of Technology and Science.

**K.Chithambaraiah Setty**

Assistant Professor  
Department of EEE,  
Bheema Institute of Technology and Science.

**Abstract:**

*Energy demand across the world is increasing and the resources are becoming scarce. The major source of power is from the conventional sources only. Some of the conventional sources of energies like thermal energy is produced from the fossil fuel coal which are depleting and is only limited to 2030. Renewable sources of energies are Solar, Wind, Biomass, etc hold bright prospect for the future.*

*In this paper simulation of Hybrid wind and solar energy supply system, in wind using self-excited induction generator (SEIG) is done.*

**I.INTRODUCTION**

Renewable energy sources, such as wind energy and photovoltaic (PV) energy, are used by stand-alone systems supplying remote houses. These sources are of intermittent nature and, therefore, the stand-alone systems should include storage battery banks. The storage battery banks improve the reliability of these systems because the excess energy is stored in the battery bank, and this energy is delivered to the load when the available energy is not sufficient.

Wind energy and photovoltaic energy have complementary characters. Combining wind energy and photovoltaic in one system (hybrid system) increases the reliability of this system and reduces the storage batteries [1]–[4].

The general configuration of stand-alone hybrid wind-PV system with battery storage is shown in Fig. 1, where the generator used by the wind subsystem is a

permanent-magnet synchronous generator (PMSG) [1], [5], [6].

Compared to induction generator, PMSG is sensitive to heat and of high cost. However, stand-alone hybrid wind-PV system with battery storage using induction generator is not investigated in the literature.

In this paper, it is proposed to use squirrel-cage induction generator (SCIG) instead of PMSG, and to use direct torque control (DTC) technique in the wind subsystem. This controlled generator is used in collaboration with the PV unit to build the stand-alone hybrid system. It is commonly known that there is a maximum voltage limit of the battery bank to protect the battery bank against overcharging [6]–[9]. Therefore, it is required to capture the maximum power from the renewable energy source provided that the maximum voltage limit is not exceeded [6]. The Voltage constraint will be followed in this paper to determine the load sharing of the PV and wind energy subsystems.

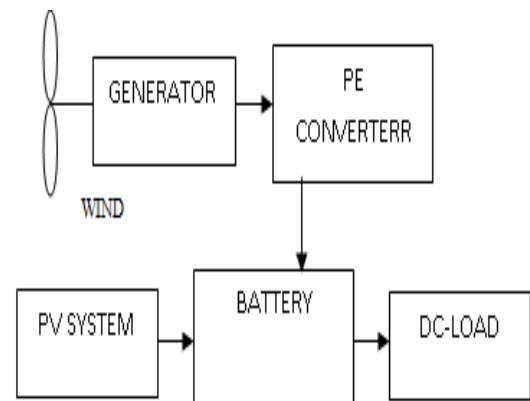


**Fig. 1** General configuration of stand-alone hybrid wind-PV system.

**II. HYBRID SYSTEM**

**Photovoltaic Module:**

The Photovoltaic Module The operation and the performance of PV generator depends to its maximum power, the models describing the PV module's maximum power output behaviors are more practical for PV system assessment. The following section describes the mathematical model for estimating the power output of PV. The equivalent circuit of a PV cell is shown in Fig 2. It includes a current source, a diode, a series resistance and a shunt resistance [2], [4].

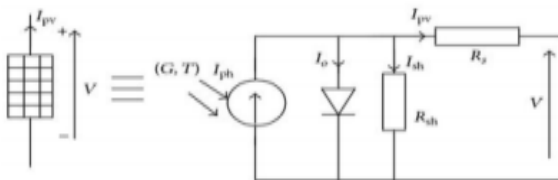


**Fig. 2 The equivalent circuit of a PV cell**

The current source Iph represents the cell photocurrent. Rsh and Rs are the intrinsic shunt and series resistances of the cell, respectively. Usually the value of Rsh is very large and that of Rs is very small, hence they may be neglected to simplify the analysis. PV cells are grouped in larger units called PV modules which are further interconnected in a parallel-series configuration to form PV arrays. The photovoltaic panel can be modeled mathematically as given in equations below: Module photo-current:

$$I_{ph} = [I_{SCr} + K_i (T - 298)] * G / 1000 \quad (1)$$

Where Iph is the light generated current in a PV module (A), ISCr is the PV module short-circuit current at 25oC and 1000W/m2 , Ki is the short-circuit current temperature co-efficient at ISCr = 0.0017A=oC, T is the module operating temperature in Kelvin, G is the PV module illumination (W/m2 ) = 1000W/m2 .

Module reverses saturation current - Irs:

$$I_{rs} = I_{scR} [e( V_o C N_s k A T) - 1] \quad (2)$$

Where q is Electron charge = 1.610-19C, Voc is the open circuit voltage, Ns is the number of cells connected in series, k is Boltzman constant = 1.3805\*10 -23J/K, A = B is an ideality factor = 1.6,

The module saturation current Io varies with the cell temperature, which is given by

$$I_o = I_{rs} [T T_r]^{-3} e^{*E_{go} B k [1 T_r - 1 T]} \quad (3)$$

Where Tr is the reference temperature = 298 K, Io is the PV module saturation current (A), Ego is the band gap for silicon = 1.1 eV.

The current output of PV module is

$$I_{pv} = N_p * I_{ph} - N_p * I_o [exp [q * (V_{pv} + I_{pv} R_s) / N_s A] - 1] \quad (4)$$

Where Np is the number of cells connected in parallel, Vpv is output voltage of a PV module (V), Ipv is output current of a PV module (A), Rs is the series resistance of a PV module. Equations (1) - (4) are used to develop the PV model.

**The Wind Turbine:**

Currently two types of configuration for wind turbine exist, which is the vertical-axis wind turbine (VAWT) configuration and the widely used horizontal axis wind turbine (HAWT) configuration. HAWT have the ability to collect maximum amount of wind energy for time of day and season and their blades can be adjusted to avoid high wind storm. Wind turbines operate in two modes namely constant or variable speed. For a constant speed turbine, the rotor turns at constant angular speed regardless of wind variations. One advantage of this mode is that it eliminates expensive power electronics such as inverters and converters. Its disadvantage however, is that it constrains rotor speed so that the turbine cannot operate at its peak efficiency in all wind speeds. For this reason a constant wind speed turbine produces less energy at low wind speeds than does a variable wind speed turbine which is designed to operate at a rotor speed proportional to the wind speed below its rated wind speed [3]. The output power or torque of a wind

turbine is determined by several factors. Among them are (i) turbine speed, (ii) rotor blade tilt, (iii) rotor blade pitch angle (iv) size and shape of turbine, (v) area of turbine, (vi) rotor geometry whether it is a HAWT or a VAWT, (vii) and wind speed. A relationship between the output power and the various variables constitute the mathematical model of the wind turbine. In this paper a model describing HAWT is proposed.

For an object having mass  $m$  and velocity  $V$  under a constant acceleration, the kinetic energy  $W_w$  is given by

$$W_w = 1/2 mv^2 \quad (5)$$

The power  $P_w$  in the wind is given by the rate of change of kinetic energy, i.e

$$P_w = dW_w / dt = 1/2 dm / dt V_w^2 \quad (6)$$

But the mass flow rate is given by

$$dm / dt = \rho A V_w \quad (7)$$

Where  $A$  is the swept area of the turbine,  $\rho$  is the density of air. With this expression equation (7) becomes

$$P_w = 1/2 \rho A V_w^3 \quad (8)$$

The actual mechanical power  $P_w$  extracted by the rotor blades in watts is the difference between the upstream and the downstream wind powers [3], i.e.

$$P_w = 1/2 \rho A V_w (V_u^2 - V_d^2) \quad (9)$$

Where  $V_u$  is the upstream wind velocity at the entrance of the rotor blades in m/s and  $V_d$  is the downstream wind velocity at the exit of the rotor blades in m/s. From the mass flow rate, the equation can be written as

$$\rho A V_w = \rho A (V_u + V_d)^2 \quad (10)$$

$V_w$  being the average of the velocities at the entry and exit of rotor blades of turbine. With this expression, equation (10) can be simplified and becomes

$$P_w = 1/2 \rho A V_w^3 \quad (11)$$

Where  $C_p$  is a fraction called the power coefficient. The power coefficient represents a fraction of the power in the wind captured by the turbine and has a theoretical maximum of 0.593.  $C_p$  is often called the Betz limit after the Germany physicist Albert Betz who worked it out in 1919. The power coefficient can be expressed by a typical empirical formula as

$$C_p = 1/2 (\lambda - 0.022\beta^2 - 5.6)e^{-0.17} \quad (12)$$

Where  $\beta$  is the pitch angle of the blade in degrees and  $\lambda$  is the tip speed ratio of the turbine, defined as

$$\lambda = V_w(\text{mph}) / w_b \text{ (rads}^{-1}\text{)} \quad (13)$$

Where  $w_b$  is the turbine angular speed. Equations (5) - (13) describe the power captured by the turbine and constitute the turbine model.

#### **Energy storage system (Battery):**

The harnessing of renewable energies presents, however, a further set of technical and economic problems. Unlike fossil and nuclear fuels, which are concentrated sources of energy that can be easily stored and transported, renewable forms of energy are highly dilute and diffuse. Moreover, their supply can be extremely intermittent and unreliable. So, batteries are required to even out irregularities in the solar and wind power distributions.

The development of battery behavior models has been the focus of researchers for many years. Based on the model given by Gu H et al [5] and incorporation of the diffusion precipitation mechanism studied by Ekdunge and Simonsson [6] in the reaction kinetics of the negative electrode, Kim and Hong [7] analyzed the discharge performance of a flooded lead acid battery cell using mathematical modeling. Bernardi and Carpenter [8] developed a mathematical model of lead acid batteries by adding the oxygen recombination reaction. Nguyen et al. [9] presented a model analogous to the flooded type and examined the dynamic behavior of the cell during discharge with respect to cold cranking amperage and reserve capacity. In general, these models are complex in terms of the expressions and number of parameters

employed. Yang et al. [10] states that a lead acid battery is characterized by two indexes, i.e. the state of charge (SOC) and the floating charge voltage (or the terminal voltage). Extensive SOC determination methods have been introduced by Sabine Piller et al. [11]. It concluded that the most used modeling technique at this time for all systems is ampere-hour counting method because it is the most direct and transparent method and quite easily implemented with satisfyingly accurate results for short-time applications, especially if used in the range of low to medium SOC. The lead-acid battery is proposed in this paper for energy storage. The section below describes the mathematical formulation of lead acid battery model based on its state of charge.

At any hour the state of battery is related to the previous state of charge and to the energy production and consumption situation of the system during the time from  $t-1$  to  $t$ . During the charging process, when the total output of PV and wind generators is greater than the load demand, the available battery bank capacity at hour  $t$  can be described by [12].

$$C_{bat}(t) = C_{bat}(t-1) (1 - \sigma) + (E_{pv}(t) + E_{WG}(t) - EL(t) / \eta_{inv}) \eta_{bat} \quad (14)$$

On the other hand, when the load demand is greater than the available energy generated, the battery bank is in discharging state. Therefore, the available battery bank capacity at hour  $t$  can be expressed as

$$C_{bat}(t) = C_{bat}(t-1) * (1 - \sigma) - (EL(t) \eta_{inv} - E_{pv}(t) + E_{WG}(t)) \quad (15)$$

Where  $C_{bat}(t)$  and  $C_{bat}(t-1)$  are the available battery bank capacity (Wh) at hour  $t$  and  $t-1$ , respectively,  $\eta_{bat}$  is the battery efficiency (During discharging process, the battery efficiency = 1)  $\sigma$  is self-discharge rate of the battery bank.  $E_{pv}(t)$  and  $E_{WG}(t)$  are the energy generated by PV and wind generators, respectively;  $EL(t)$  is the load demand at hour  $t$  and  $\eta_{inv}$  is the inverter efficiency [%] At any hour, the storage capacity is subject to the following constraints:

$$C_{batmin} \leq C_{bat}(t) \leq C_{batmax} \quad (16)$$

### III. CONTROL STRATEGY FOR STAND-ALONE WIND SYSTEM

The wind flow is erratic in nature. Therefore, a WECS is integrated with the load by means of an ac-dc-dc converter to avoid voltage flicker and harmonic generation. The control scheme for a stand-alone hybrid wind-battery system includes the charge controller circuit for battery banks and pitch control logic to ensure WT operation within the rated value. The control logic ensures effective control of the WECS against all possible disturbances.

#### A. Charge Controller for the Battery Bank

This section discusses in detail the development of charge controller circuit for a 400 Ah, C/10 battery bank using a dc-dc buck converter in MATLAB/SIMULINK platform. Generally, the batteries are charged at C/20, C/10, or C/5 rates depending on the manufacturer's specification where C specifies the Ah rating of battery banks. So, the battery bank system considered in the design can be charged at 20, 40, or 80 A. But, in this paper, C/10 rate (i.e., 40 A) for battery charging is chosen. However, the current required for charging the battery bank depends on the battery SoC. A typical battery generally charges at a constant current (CC), i.e., C/10 rate mode till battery SoC reaches a certain level (90%–98%). This is referred to as CC mode of battery charging. The CC mode charges the battery as fast as possible. Beyond this SoC, the battery is charged at a constant voltage (CV) which is denoted as CV mode of battery charging in order to maintain the battery terminal voltage.

#### B. Control Strategy

The implementation of the charge control logic as shown in Fig. 2 is carried out by three nested control loops. The outer most control loop operates the turbine following MPPT logic with battery SoC limit. To implement the MPPT logic, the actual tip speed ratio (TSR) of turbine is compared with the optimum value. The error is tuned by a PI controller to generate the battery current demand as long as the battery SoC is below the CC mode limit. Beyond this point, the SoC

control logic tries to maintain constant battery charging voltage. This in turn reduces the battery current demand and thus prevents the battery bank from overcharging. The buck converter inductor current command is generated in the intermediate control loop. To design the controller, it is essential to model the response of the battery current ( $I_b$ ) with respect to the inductor current ( $I_L$ ).

This article has been accepted for inclusion in a future issue of this journal. Content is final as presented, with the exception of pagination.

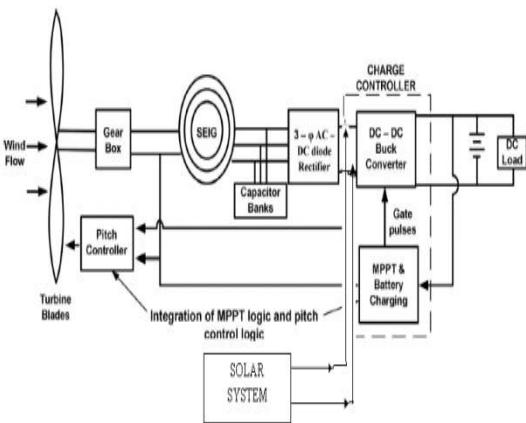


Fig. 1. Layout of hybrid wind-battery system for a stand-alone dc load.

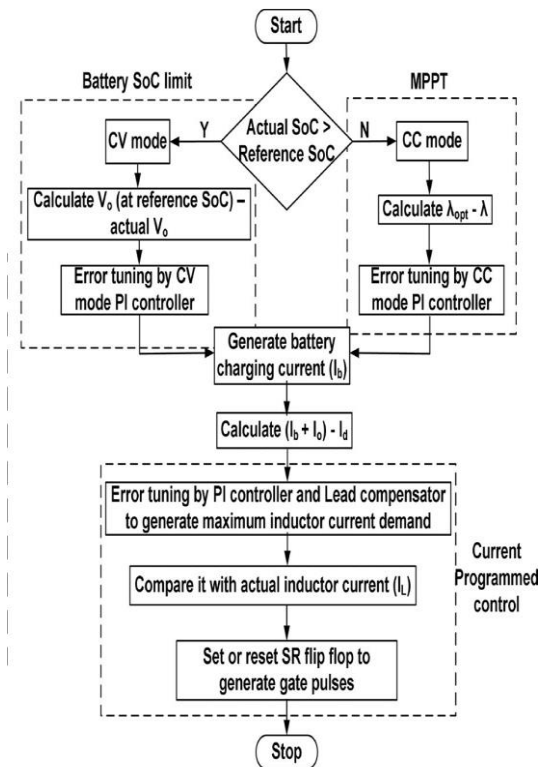


Fig. 2. Block schematic and flowchart of the charge controller circuit for battery.

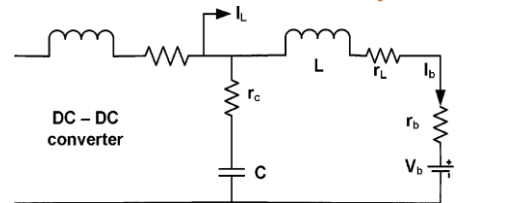
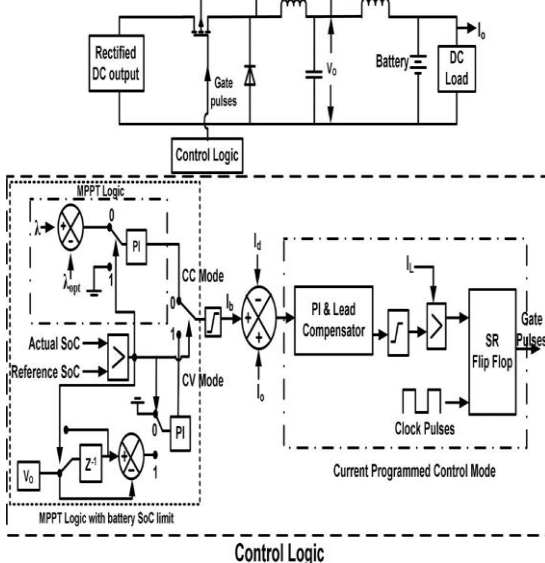


Fig. 3. Circuit representation of buck converter output.

The transfer function can be computed from Fig. 3 and is given by (1)

As shown in Fig. 3, the battery is assumed to be a CV source with a small internal resistance ( $r_b$ ). The effective series resistances (ESR) of the capacitor ( $r_c$ ) and the inductor ( $rL$ ) are also considered. The ESR of the capacitor and the inductor is taken to be  $1m\Omega$  each. The battery internal resistance is  $10\text{ m}\Omega$ . For regulating the peak-to-peak (p-p) ripple of battery current and converter output voltage within 2% of the rated value the L and C are calculated to be  $10\text{ mH}$  and  $5\text{ mF}$ , respectively.



For controlling the battery current the actual converter output current ( $I_d$ ) is compared with the reference ( $I_b + I_a$ ) and the error is processed by a cascade of a PI and a lead compensator. The PI controller is modeled as an inverted zero. To maintain the phase margin of the open-loop system the frequency of this zero is 50 times lower than the crossover frequency. To improve the phase margin of the battery charging current control loop (i.e., (1) along with the PI controller) a lead compensator is connected in cascade with the PI controller as shown in Fig. 2.

The zero and pole of the lead compensator are designed to have a positive phase margin and to restrict the crossover frequency to about 14% of the switching frequency. The bode plot of the PI controller along with the lead compensator and the loop gain of the battery current control loop are shown in Fig. 4(a) and (b). As shown in Fig. 4, the phase margin is  $34.2^\circ$  at 130 Hz. The output of the lead compensator determines inductor current reference for the dc–dc converter.

In order to prevent over loading the turbine (and its consequent stalling) the lead compensator output is first passed through an adjustable current limiter.

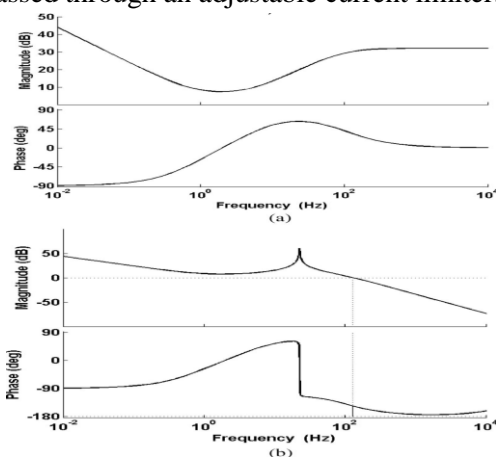


Fig. 4. Bode plot of (a) PI controller in cascade with lead compensator. (b) Loop gain of the battery current control loop.

The lower limit is set to zero and the upper limit is varied according to the maximum power available at a

given wind speed. The output of this limiter is used as the reference for the current controller in the dc–dc converter.

Finally, in the inner most loop the actual inductor current is made to track the reference using peak current mode control [21]. The compensated output of the intermediate loop is compared with the instantaneous inductor current of the buck converter. The output of the comparator is applied to an SR flip flop to produce the gate pulses for the dc–dc buck converter. The frequency of the clock pulses is 2 kHz. The frequency of the gate pulse is equal to the clock pulse frequency. This method of generating gate pulses for the converter is known as the current programmed control technique. The advantage of this method is that it does not allow the inductor current to go beyond the rated limit. This in turn protects the buck converter switch and inductor from over current situation.

### Generator Side Converter Control

The mechanical power captured from wind turbine is governed by the following equation:

$$P_m = 0.5 \rho A C_p v_w^3 \quad (1)$$

Where  $P_m$  is the mechanical output power of the wind turbine (Watt),  $\rho$  is the Air density ( $\text{Kg/m}^3$ ),  $A$  is the swept area ( $\text{m}^2$ ),  $C_p$  is the power coefficient of the wind turbine and  $v_w$  is the wind speed (m/second). Consequently, the output energy is determined by the power coefficient ( $C_p$ ) of wind turbine if the swept area, air density, and wind speed are assumed to be constant.  $C_p$  is function in tip speed ratio ( $\lambda$ ) and pitch angle ( $\beta$ ) in degree. If  $\beta$  is equal zero, in this case  $C_p$  is only function in  $\lambda$  as shown in (2), and  $\lambda$  is function of rotor mechanical speed, rotor radius of blade and wind speed as indicated in (3).

$$C_p(\lambda) = \frac{60.04 - 4.69\lambda}{\lambda} e^{\left(\frac{-21 + 0.735\lambda}{\lambda}\right)} + \frac{0.0068\lambda}{1 - 0.035\lambda} \quad (2)$$

$$\lambda = \frac{\omega_r R}{v_w} \quad (3)$$

Where  $\omega_r$  is the rotational speed (rad/second) and  $R$  is the radius of blade (m). The relation between  $C_p$  and  $\lambda$

when  $\beta$  equal zero degree is shown in Figure 2. It can be noticed that the optimum value of  $C_p$  is about 0.48 for  $\lambda$  equal 8.1. Maximum power extraction from wind turbine can be achieved when the turbine operate at maximum  $C_p$  ( $C_{p-opt}$ ). Therefore, it is necessary to adjust the rotor speed at optimum value of tip speed ratio ( $\lambda_{opt}$ ) with wind speed variation.

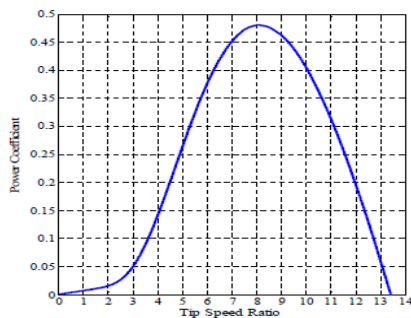


**Figure 2.**The relation between power coefficient ( $C_p$ ) and tip speed ratio ( $\lambda$ ).

Using (1) and (3), the optimum output power from wind turbine can be written as:

$$P_{m\_opt} = 0.5 \rho A C_{p\_opt} \left( \frac{\omega_{r\_opt} R}{\lambda_{opt}} \right)^3 = K_{opt} (\omega_{r\_opt})^3 \quad (4)$$

Where

$$K_{opt} = 0.5 \rho A C_{p\_opt} \left( \frac{R}{\lambda_{opt}} \right)^3 \quad (5)$$

$$\omega_{r\_opt} = \frac{\lambda_{opt}}{R} v_w = K_{\omega} v_w \quad (6)$$

Figure 3 indicates that the mechanical powers generated by the turbine as a function of rotor speeds for different wind speeds. The maximum power extraction within the allowable range can be achieved if the controller can properly follow the optimum curve with variation of wind speed.

The generator side converter (a single switch three phase mode rectifier) is controlled to extract maximum power from available wind turbine power. Hence, the wind turbine can produce maximum power when the turbine operates at optimum value of  $C_p$  ( $C_{p-opt}$ ). So it is necessary to adjust the rotor speed at optimum value of the tip speed ratio ( $\lambda_{opt}$ ).

### C. Pitch Control Mechanism

The WT power output is proportional to the cube of wind velocity [15]. Generally the cut-off wind speed of a modern WT is much higher compared to the rated wind speed [9]. If the WT is allowed to operate over the entire range of wind speed without implementation of any control mechanism, the angular speed of the shaft exceeds its rated value which may lead to damage of the blades. So, it is very much essential to control the speed and power at wind speeds above the rated wind speed.

This is achieved by changing the pitch angle of the blade. Such a mechanism is referred to as the pitch control of WT. The power coefficient ( $C_p$ ) versus TSR ( $\lambda$ ) characteristics of the WT considered in this study for different pitch angles are shown in Fig. 6. As examined from the characteristics, at a pitch angle of zero degree the value of  $C_p$  is maxima. But the optimum value of power coefficient reduces with increase in pitch angle. This happens because with increase in blade pitch the lift coefficient reduces which results in decreasing the value of  $C_p$  [15]. So, the pitch control mechanism controls the power output by reducing the power coefficient at higher wind speeds.

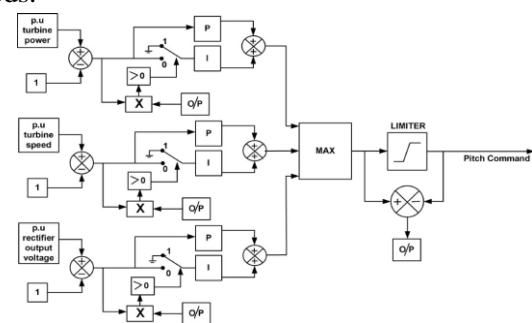


**Fig. 7.** Pitch control scheme for a stand-alone WECS.

Below the rated wind speed the blade pitch is maintained at zero degree to obtain maximum power. The pitch controller increases the blade pitch as the WT parameters exceed the rated value. The reduction in the value of  $C_p$  by pitching compensates for the increase in WT power output under the influence of higher wind speeds. Apart from regulating the WT

parameters, it is also essential to control the output voltage of the ac–dc rectifier to avoid overvoltage condition in the WECS. Hence, the pitch controller ensures that with desirable pitch command, the WT parameters and the rectifier output dc voltage are regulated within their respective maximum allowable limits to ensure safe operation of the WECS.

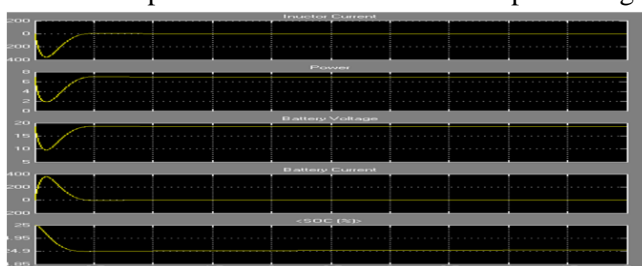
### D. Pitch Control Scheme

The pitch control scheme is shown in Fig. 7. As seen the p.u. value of each input is compared with 1 to calculate the error. The errors are tuned by PI controller. The “MAX” block chooses the maximum output from each PI controller which is then passed on to a limiter to generate the pitch command for the WT. The actual pitch command is compared with the limited value. The lower limit of the pitch command is set at zero.

There arises an error when the actual pitch command goes above or below the specified limit. This is multiplied with the error obtained from each of the comparator. The product is compared with zero to determine the switching logic for integrator. This technique is carried out to avoid integrator saturation. The pitch controller changes the pitch command owing to variation in turbine rotation speed, power, and output voltage of rectifier, which ensures safe operation of the WECS.

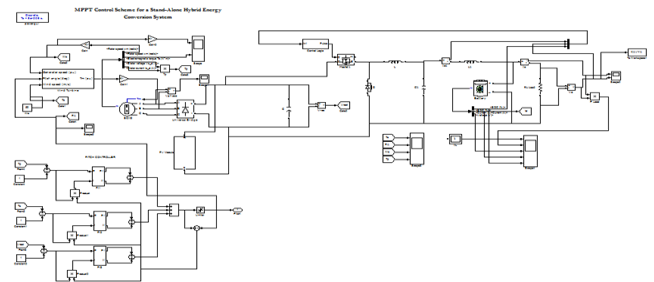
## VI. SIMULATION RESULTS

Simulation is performed using MATLAB/SIMULINK software. Simulink library files include inbuilt models of many electrical and electronics components and devices such as diodes, MOSFETS, capacitors, inductors, motors, power supplies and so on. The circuit components are connected as per design



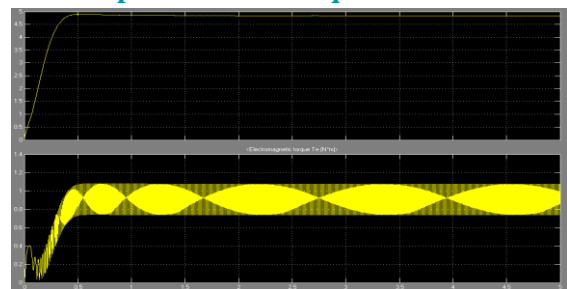
without error, parameters of all components are configured as per requirement and simulation is performed

### SIMULATION CIRCUIT

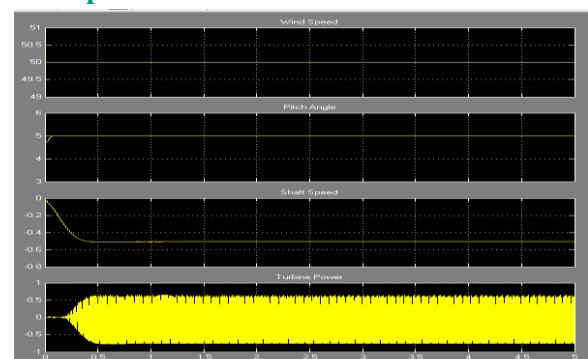


### WAVEFORMS

#### Generator Speed & EM Torque



#### Turbine parameters



### CONCLUSION

Performance of stand-alone hybrid wind-PV system with battery storage is studied. The proposed wind subsystem using SCIG and DTC technique is studied. The reactive power required by SCIG is obtained from the battery bank through PWM rectifier. According to the battery-bank voltage (udc), there are two modes of operation of the system. One mode when the battery-

bank voltage is less than or equal to the maximum voltage limit, and the other mode when the battery bank voltage exceeds the maximum voltage limit. In the first mode, the battery-bank voltage is below its maximum value, and thus the PV and wind subsystems are allowed to follow their maximum powers. In the second mode, the captured power is limited such that the battery bank voltage does not exceed its maximum value.

Modeling and control of the system are demonstrated. Good performance of the system is verified by the results obtained for each mode of operation. The hybrid system along with its control logic is developed in MATLAB/SIMULINK and is tested with various wind profiles. The outcome of the simulation experiments validates the improved performance of the system.

## REFERENCES

- [1] A. D. Sahin, "Progress and recent trends in wind energy," *Progress in Energy Combustion Sci.*, vol. 30, no. 5, pp. 501–543, 2004.
- [2] R. D. Richardson and G. M. Mcnerney, "Wind energy systems," *Proc. IEEE*, vol. 81, no. 3, pp. 378–389, Mar. 1993.
- [3] R. Saidur, M. R. Islam, N. A. Rahim, and K. H. Solangi, "A review on global wind energy policy," *Renewable Sustainable Energy Rev.*, vol. 14, no. 7, pp. 1744–1762, Sep. 2010.
- [4] M. T. Ameli, S. Moslehpur, and A. Mirzale, "Feasibility study for replacing asynchronous generators with synchronous generators in wind farm power stations," in *Proc. IAJC – IJME, Int. Conf. Eng. Technol., Music City Sheraton, Nashville, TN, US, ENT paper 129Nov. 17–19, 2008.*
- [5] G. K. Singh, "Self excited generator research—A survey," *Electric Power Syst. Res.*, vol. 69, no. 2/3, pp. 107–114, 2004.
- [6] R. C. Bansal, "Three-phase self-excited induction generators: An overview," *IEEE Trans. Energy Convers.*, vol. 20, no. 2, pp. 292–299, Jun. 2005.
- [7] S. C. Tripathy, M. Kalantar, and N. D. Rao, "Wind turbine driven self excited induction generator," *Energy Convers. Manag.*, vol. 34, no. 8, pp. 641–648, 1993.
- [8] A. Chakraborty, "Advancements in power electronics and drives in interface with growing renewable energy resources," *Renewable Sustainable Energy Rev.*, vol. 15, no. 4, pp. 1816–1827, May 2011.
- [9] F. D. Gonz´alez, A. Sumper, O. G. Bellmunt, and R. V. Robles, "A review of energy storage technologies for wind power applications," *Renewable Sustainable Energy Rev.*, vol. 16, no. 4, pp. 2154–2171, May 2012.
- [10] N. S. Hasan, M. Y. Hassan, M. S. Majid, and H. A. Rahman, "Review of storage schemes for wind energy systems," *Renewable Sustainable Energy Rev.*, vol. 21, pp. 237–247, May 2013.
- [11] A. M. D. Broe, S. Drouilhet, and V. Gevorgian, "A peak power tracker for small wind turbines in battery charging applications," *IEEE Trans. Energy Convers.*, vol. 14, no. 4, pp. 1630–1635, Dec. 1999.
- [12] R. Kot, M. Rolak, and M. Malinowski, "Comparison of maximum peak power tracking algorithms for a small wind turbine," *Math.Comput.Simul.*, vol. 91, pp. 29–40, 2013.
- [13] M. Narayana, G. A. Putrus, M. Jovanovic, P. S. Leung, and S. McDonald, "Generic maximum power point tracking controller for small-scale wind turbines," *Renewable Energy*, vol. 44, pp. 72–79, Aug. 2012.
- [14] K. Y. Lo, Y. M. Chen, and Y. R. Chang, "MPPT battery charger for standalone wind power system,"



IEEE Trans. Power Electron., vol. 26, no. 6, pp. 1631–1638, Jun. 2011.

[15] E. Hau, Wind Turbines Fundamentals, Technologies, Application, Economics, 2nd ed. New York, NY, USA: Springer, Dec. 2005.

[16] Aradhya Sambhu Satpathy, N. K. Kishore, Senior Member, IEEE, Debaprasad Kastha, Member, IEEE, and N. C. Sahoo, Member, IEEE